



# Comparative efficacy of histogram-based local descriptors and CNNs in the MRI-based multidimensional feature space for the differential diagnosis of Alzheimer’s disease: a computational neuroimaging approach

Egils Avots<sup>1</sup> · Akbar A. Jafari<sup>1</sup> · Cagri Ozcinar<sup>1</sup> · Gholamreza Anbarjafari<sup>1,2,3,4</sup> ·  
for the Alzheimer’s Disease Neuroimaging Initiative

Received: 13 October 2023 / Revised: 10 November 2023 / Accepted: 5 December 2023 / Published online: 25 February 2024  
© The Author(s), under exclusive licence to Springer-Verlag London Ltd., part of Springer Nature 2024

## Abstract

The utilisation of magnetic resonance imaging (MRI) images for the automated detection of Alzheimer’s disease has garnered significant attention in recent years. This interest stems from the progress made in machine learning techniques and the possible application of such methods in the field of diagnostics. This study aims to evaluate the performance of 16 histogram-based image texture descriptors and features extracted from 18 pre-trained convolutional neural networks in characterising brain patterns observed in 2D slices of MRI images. The primary objective is to determine the most effective feature types for this task. The characteristics were taken from the magnetic resonance imaging (MRI) dataset given by the Alzheimer’s Disease Neuroimaging Initiative (ADNI). The study involved the calculation of features on 2D axial, coronal, and sagittal slices, followed by classification using five binary machine learning algorithms. The objective was to differentiate between individuals with normal cognitive function and those diagnosed with Alzheimer’s disease. The proposed methodology additionally facilitated the identification of specific brain areas to be selected for each axis, in order to achieve optimal accuracy. This involved determining the matching feature and classifier combinations.

**Keywords** Alzheimer’s disease · Magnetic resonance imaging (MRI) · Feature extraction · Machine learning · ADNI

---

Data used in preparation of this article were obtained from the Alzheimer’s Disease Neuroimaging Initiative (ADNI) database (adni.loni.usc.edu). As such, the investigators within the ADNI contributed to the design and implementation of ADNI and/or provided data but did not participate in analysis or writing of this report. A complete listing of ADNI investigators can be found at: [http://adni.loni.usc.edu/wp-content/uploads/how\\_to\\_apply/ADNI\\_Acknowledgement\\_List.pdf](http://adni.loni.usc.edu/wp-content/uploads/how_to_apply/ADNI_Acknowledgement_List.pdf).

---

✉ Egils Avots  
egils@ut.ee

Akbar A. Jafari  
akbar.anbarjafari@ut.ee

Cagri Ozcinar  
chagri.oachinar@ut.ee

Gholamreza Anbarjafari  
shb@ut.ee

<sup>1</sup> iCV Research Lab, Institute of Technology, University of Tartu, Tartu, Estonia

<sup>2</sup> iVCV OÜ, Tartu, Estonia

## 1 Introduction

The study of diseases related to cognitive decline is particularly important as there are over 50 million people worldwide living with dementia in 2020, and it is predicted that this number will almost double every 20 years, reaching 82 million in 2030 [1]. Dementia is a general term for a decline in mental ability severe enough to interfere with daily life. It can be a chronic or persistent disorder of the mental processes caused by brain disease or injury and marked by memory disorders, personality changes, and impaired reasoning. Alzheimer’s, which is the most common cause of dementia, accounting for 60–80% of dementia cases, is a type of dementia that causes problems with decline in memory, reasoning, and behaviour. As there is no cure for Alzheimer’s disease, modern medicine

<sup>3</sup> Faculty of Engineering, Yildiz Technical University, Istanbul, Turkey

<sup>4</sup> PwC Advisory, Helsinki, Finland

is focused on the prevention of early-onset Alzheimer's and symptom management [2–5]. While differentiating between healthy patients and patients with Alzheimer's disease is useful for gathering knowledge about the disease and tailoring the individual's medical treatment, from the patient's perspective, it may already be too late. The first onset of mild cognitive impairment (MCI) and later stages of cognitive decline are diagnosed using various psychological tests, such as the famous clock test [6] or other methods such as physical exams, neurological exams, mental status tests, mood assessments, genetic testing, and brain imaging.

The first indications of progressing Alzheimer's can express themselves as MCI, which can last from 2 to 7 years, according to the Global Deterioration Scale. By diagnosing MCI in a timely manner, the patient can start preventive measures and delay the onset of later stages of cognitive decline. Lately, deep learning is being used in brain imaging such as magnetic resonance imaging (MRI) and positron emission tomography (PET) scans to detect Alzheimer's and even MCI, where the ultimate goal is to predict the risk of developing MCI and Alzheimer's years before they develop. Until the wide acceptance of deep learning, various visual descriptors were used to classify MRI images. These descriptors were based on image texture descriptors used in computer vision and modified for MRI images. Using this approach, researchers are trying to invent visual descriptors that would outperform their predecessors.

Nowadays, due to advances in computing power, neural networks offer state-of-the-art classification capabilities for image processing tasks [7–10]. This shift in technology suggests that the time and effort spent on handcrafting visual descriptors might be over. For example, a neural network can be trained from scratch with enough input data; an easier approach is to use pre-trained neural networks, referred to as transfer learning, where the weights of the network are initialised based on networks that have been trained on millions of images and the end of the network is changed according to the problem at hand. Similarly, the feature extraction part of a neural network can be combined with a classifier, such as a support vector machine (SVM).

The main contribution of this study is the exploration of different histogram-based features and features extracted from pre-trained CNNs used on brain MRI data and their usefulness for diagnosis ascertained through an exhaustive search among different MRI slice, feature, and classifier combinations. The proposed framework is based on feature preparation for the classification of cognitively normal (CN) and Alzheimer's disease (AD) patients from the selection of 2D slices of the MRI scans.

## 2 Features for image classification

### 2.1 Histogram-based local descriptors

Local descriptors based on histograms [11–13] have been shown to be effective tools for feature extraction and image analysis. With the ability to identify regional patterns and spatial information, these descriptors provide a condensed representation of image features. Histogram-based local descriptors for MRI help with image segmentation, registration, and classification tasks by offering insights into local intensity variations and textural patterns.

Histogram-based local descriptors examine how voxel intensities are distributed locally within an MRI image. They characterise the statistical characteristics of the intensities and are often estimated within local neighbourhoods or regions of interest (ROIs). Important characteristics include intensity changes, texture patterns, and spatial interactions between adjacent voxels.

Histogram-based local descriptors offer several benefits, which can be summarised below:

- They are insensitive to global image transformations such as translation, rotation, and scaling, making them resistant to variations in viewpoint.
- They are computationally efficient because histograms can be independently and concurrently computed.
- The histograms are adaptable to varying illumination conditions, which increases their resilience.
- Histogram-based descriptors are appropriate for large-scale image databases because they are compact and easily stored.

Notably, the most widely used histogram-based local descriptors in medical imaging are local binary pattern (LBP), histogram of gradients (HOG), and local phase quantization (LPQ). To expand on this topic, the potential use of 16 histogram-based local descriptors (as shown in Table 1) is examined and their performance is evaluated in brain MRI classification. The credit for method implementation in MATLAB goes to Turan and Lam [12], who investigated local descriptor performance for facial expression recognition.

### 2.2 Pre-trained convolutional neural networks

Pre-trained convolutional neural networks (CNNs) are potent computer vision tools that have been trained to extract meaningful features from images using large datasets such as

**Table 1** Histogram-based local descriptors

Nr.	Abbrev.	Descriptor Name	Dim.
1	LBP [14]	Local Binary (Bin.) Pattern	59
2	HOG [15]	Hist. of Oriented Gradients	6084
3	PHOG [16]	Pyramid of Hist. of Oriented Gradients	168
4	LPQ [17–19]	Local Phase Quantization	256
5	LMP [20]	Local Monotonic Pat.	256
6	LTrP [21, 22]	Local Transitional Pat.	256
7	MBC [23, 24]	Monogenic Bin. Coding	3072
8	LGIP [25]	Local Gradient Increasing Pat.	37
9	LDN [26]	Local Directional Number Pat.	56
10	GDP [27–29]	Gradient Directional Pat.	256
11	WLD [30, 31]	Weber Local Descriptor	32
12	LAP [32]	Local Arc Pattern	272
13	LGP [33]	Local Gradient Pattern	7
14	MBP [34]	Median Bin. Pattern	256
15	LDTP [35]	Local Directional Texture Pat.	72
16	IWBC [36]	Improved Weber Bin. Coding	2048

**Table 2** Pre-trained convolutional neural networks

Nr.	Network	Depth	Par. (Mil.)	Dim.
1	AlexNet [41]	8	62.3	4096
2	VGG16 [42]	16	138	4096
3	VGG19 [42]	19	144	4096
4	GoogLeNet [43]	22	7.0	1024
5	Inception-v3 [44]	48	23.9	2048
6	ResNet18 [45]	18	11.7	512
7	ResNet50 [45]	50	25.6	2048
8	ResNet101 [45]	101	44.6	2048
9	SqueezeNet [46]	18	1.24	1000
10	InceptionResNetV2 [47]	164	55.9	1536
11	Xception [48]	71	22.9	2048
12	DarkNet19 [49]	19	20.8	1000
13	DarkNet53 [49]	53	41.6	1024
14	ShuffleNet [50]	50	1.4	544
15	NASNet Mobile [51]	–	5.3	1056
16	NASNet Large [51]	–	88.9	4032
17	MobileNet-v2 [52]	53	3.5	1280
18	EfficientNet [53]	82	5.3	1280

ImageNet [37–39]. These networks have learned to recognise and categorise objects in a variety of categories, making them useful for solving a vast array of problems. By leveraging the knowledge and representations learned by these pre-trained networks, they can be used as a starting point for new image classification or recognition tasks using the transfer learning technique.

The central idea behind using pre-trained CNNs is that they can autonomously learn hierarchical image representations [40]. Earlier network layers capture low-level features

such as edges and textures, while later layers derive more complex and abstract features such as shapes and objects. These learned features can then be used to depict images in a compact and discriminatory manner, allowing for efficient feature extraction and classification.

The use of pre-trained networks and transfer learning is especially important in medical imaging due to the scarcity of data. This study demonstrates how feature extraction using pre-trained networks can be used to classify brain MRI slices and potentially eliminate the need for handcrafted feature

descriptors. The list of tested neural network models is shown in Table 2, and the models were implemented in MATLAB using MathWorks libraries and *Deep Learning Toolbox*.

### 3 Related work

The machine learning algorithms in brain imaging try to learn from the structural changes of the brain, such as reduced complexity and decreased size. For example, Nayaki and Varghese [54] used MRI scans from the Alzheimer’s Disease Neuroimaging Initiative (ADNI) database and tested local patterns of grey matter and classified them using SVM. The task of local patterns was to encode the loss of grey matter volume for MCI and AD when compared to CN. In the CN, MCI, and AD classifications, an accuracy of 76% was reached with LBP, and the best result was achieved using local quinary pattern (LQP) with an accuracy of 81%.

A study by Ben Ahmed et al. [55] also used MRI images from the ADNI dataset to divide the visual features of the hippocampi of CN, MCI, and AD patients into three groups. The experimental results show that the classification for AD versus NC subjects achieves accuracies of 87% for the ADNI subset. For MCI, they reached accuracies of 78.22% and 72.23% for MCI versus CN and MCI versus AD, respectively.

Sarwinda and Bustamam [56] proposed to use HOG features of the three orthogonal planes for the classification of AD using MRI images. The feature dimensionality was reduced using probabilistic principal component analysis (PPCA), and then random forest (RF) was used as a binary classifier to classify the features. The HOG-TOP approach achieved an accuracy of 95.8% for AD/CN, 94.4% for MCI/CN, and 93.64% for AD/MCI.

Altaf et al. [57] performed Alzheimer’s disease classification using images and clinical features based on the ADNI dataset. From image feature descriptors, they tested the grey level co-occurrence matrix (GLCM), scale invariant feature transform (SIFT), HOG, and LBP. In the case of AD vs. CN, the binary classification results of SVM, ensemble, k-nearest neighbour (KNN), and decision tree (DT) accuracy were in

the range of 50% to 60%, while other combinations such as AD/MCI and CN/MCI with GLCM reached 80% accuracy. Their proposed method reached 86.7% accuracy for CN and MCI.

Newer developments are often based on various frameworks and deep learning; for example, Cao et al. [58] combined 2D and 3D images in a MVMM learning framework, which was evaluated on the ADNI database. Their proposed model could classify MCI/CN with 87.50% accuracy and MCI/AD with 83.18% accuracy. Similarly, Cohen et al. [59] used categorical data from the ADNI dataset, which also included MRI images, to distinguish between CN, MCI, and AD with an accuracy of 87.2% using an artificial neural network (ANN) classifier and an accuracy of 88.3% using a 1D CNN classifier.

Basaia et al. [60] used CNN to predict the diagnosis of AD and MCI, which will convert to AD (c-MCI) based on a single cross-sectional brain structural MRI scan from the ADNI and Milan datasets. The learning algorithm could distinguish AD/CN with 99.2% accuracy and c-MCI/CN with 87.1% accuracy.

Table 3 presents a comparison between the use of single and multi-slice techniques in the categorization of AD, employing several machine learning algorithms.

### 4 Dataset

Data used in the preparation of this study were obtained from the Alzheimer’s Disease Neuroimaging Initiative (ADNI) database (adni.loni.usc.edu). The ADNI was launched in 2003 as a public–private partnership, led by Principal Investigator Michael W. Weiner, MD. The primary goal of ADNI has been to test whether serial magnetic resonance imaging (MRI), positron emission tomography (PET), other biological markers, and clinical and neuropsychological assessment can be combined to measure the progression of mild cognitive impairment (MCI) and early Alzheimer’s disease (AD).

The files in the ADNI1 dataset are MRI images, representing the internal structure of a patient’s head in the form of a 3D grid consisting of elements called voxels. The scans

**Table 3** Examples of state-of-the-art single- and multi-slice approach in the literature for CN/AD classification accuracy

Article	Method	Single/ multi-slice	Acc.
Nayaki & Varghese [54]	LQP+SVM	Single	81.00
Ben Ahmed et al. [55]	CHF-CSF+SVM	Single	87.00
Sarwinda et al. [56]	PPCA+RF	Multi	95.80
Altaf et al. [57]	GLCM	Single	97.80
Cao et al. [58]	MVMM	Multi	83.18
Cohen et al. [59]	1D CNN	Multi- categorical	88.30
Basaia et al. [60]	3D CNN	Multi	99.20

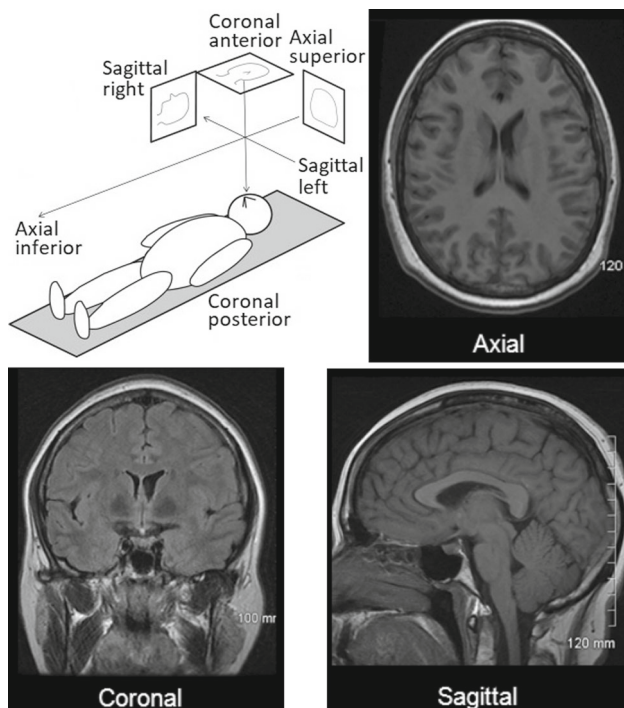


**Fig. 1** MRI slices of the axial, sagittal, and coronal planes [61]

undergo a standardised procedure and are processed using Gradwarp, B1 non-uniformity, and the N3 algorithm. The image files are stored in NIfTI format, a type of medical image format that is used to facilitate and strengthen post-processing analysis. NIfTI is a file format for neuroimaging created by a committee based at the National Institutes of Health.

The images of the patients are classified into three categories depending on the group to which they belong: cognitively normal (CN), mild cognitive impairment (MCI), and Alzheimer’s disease (AD). The used ADNI dataset subset consisted of CN and AD patients from first-year recordings done with a 1.5T MRI scanner. The dimensions of the scans had various sizes and ranged from  $192 \times 192 \times 160$  to  $256 \times 256 \times 184$ . To make use of all of the scans, the MRI scans were resized using cubic interpolation to  $224 \times 224 \times 224$ , which was the most common input image height and width for the selected CNN’s. The 2D images used in feature extraction of the MRI brain scans were created from the axial, sagittal, and coronal planes, as shown in Fig. 1.

## 5 Methodology

Using all MRI slices from each of the three orthogonal planes is possible, but such an approach requires hardware that can handle long feature vectors. A bare minimum approach is to

use one slice from one of the axes. To find out which axes are the most suitable, an exhaustive search approach was used to check all the slices. This approach also gives insight into which brain areas contain relevant features according to classification results.

The sides of MRI scans typically do not contain information about the brain; therefore, out of the 224, slices 53 to 172, in total 120, were selected for extraction in each axis. Each slice was normalised according to its minimum and maximum values and scaled to the  $[0,255]$  range to mimic the 8-bit unsigned integer data format. For the neural networks that used different input sizes, the slices were resized to match the required input dimensions.

The data samples were split according to an 80:20 train–test split, where each class had 127 patients and each patient had two recordings. In the ANDI dataset, each patient can have several MRI recordings. In our tests, the first and last recordings were selected per patient according to the MRI scan acquisition date. The data are split according to patient IDs to ensure correct training and testing data allocation and avoid the same patient appearing in both sets simultaneously.

After feature extraction, the results were classified into CN and AD. The chosen classifiers are a typical choice when creating baseline results and are available in most machine learning packages and programmes. In this study, the chosen classifiers are as follows:

- Support vector machine - Linear
- Discriminant analysis - Pseudo-linear
- Discriminant analysis - Pseudo-quadratic
- Decision tree
- K-nearest neighbour,  $k=9$

## 6 Results and discussion

The focus of this discussion is to show how well different features used on brain MRI data can be used for diagnosis and examine if brute-force machine learning model testing can find useful patterns in the brain MRI data. The analysis will specifically concentrate on three anatomical planes: axial, coronal, and sagittal.

This study investigates the effectiveness of various histogram-based features, including WLD, LAP, LDTP, and HOG, and pre-trained CNNs such as AlexNet and Dark-Net53. Our objective is to determine the model-feature combinations that obtain the highest classification accuracy. The findings are systematically recorded and analysed to uncover complex patterns and potential biomarkers that may function as crucial diagnostic criteria for neurodegenerative disorders such as AD.

Additionally, the research investigates the performance of these models on specific slices, identifying the slices that pro-

vide the highest level of discriminatory capability. The use of granular analysis is crucial for comprehending the spatial distribution of disease-specific characteristics within various brain regions. The results are consistent with prior research, which attests to the clinical importance and potential application of our computational method in the field of medical imaging and diagnosis.

### 6.1 Axial plane

When considering axial slices, the top four histogram-based features are WLD, LAP, LDTP, and HOG. According to related work, WLD has been used for intracranial haemorrhage CT classification [62] and as features for cerebral microbleed detection [63]. In computer vision, LAP is used in the field of facial expression analysis, but there are very few studies of this feature in medical imaging; for example, one study used LAP for the detection of tuberculosis using chest radiographs [64]. LDTP, which should not be confused with local variations of true phase that use the same acronym, can be found in brain tumour classification [65], mammographic breast cancer classification [66] and liver tumour segmentation [67]. The last of the top four features is HOG, which is a significantly more popular choice in medical imaging [68].

The most interesting results come from the individual slice representation. At slice number 88, you can see the peak from the histogram descriptors (see Fig. 2), and the pre-trained networks make a curve that looks like the top of a Gaussian distribution around a nearby point (see Fig. 3). The axial view of these slices is slicing through *Corpus Callosum* or slightly above it. Different patterns of cortical atrophy help to tell the difference between dementias like AD. For example,

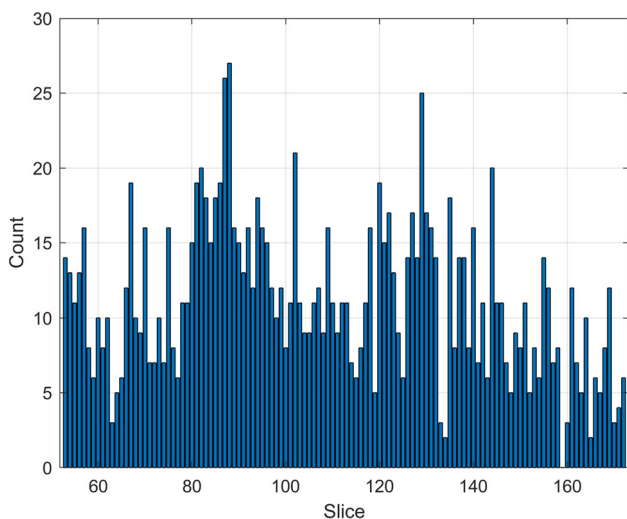


**Fig. 2** Axial plane: Slice histogram for histogram descriptors. Slices are ordered from top to bottom of the patient’s head

the mean surface area of the corpus callosum is much smaller in Alzheimer’s patients than in healthy controls [69].

Table 4 primarily examines the axial plane and utilises a range of histogram-based features for the classification of CN/AD. According to the data presented in the table, it can be observed that the integration of the WLD feature with SVM and LDA classifiers yields the highest accuracy rate of 72.22%. This finding implies that the WLD feature exhibits strong resilience in accurately classifying individuals with normal cognition and Alzheimer’s disease in the axial plane.

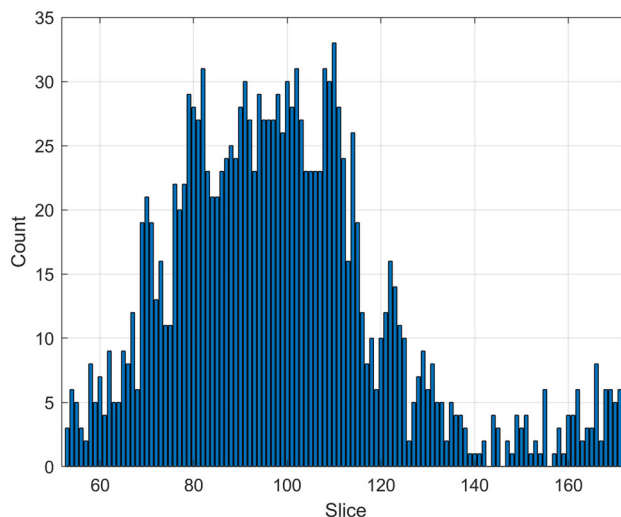


**Fig. 3** Axial plane: Slice histogram for pre-trained CNN features. Slices are ordered from top to bottom of the patient’s head

**Table 4** Best axial CN/AD classification results using histogram descriptors

Features	SVM	LDA	QDA	DT	KNN
GDP	62.04	64.81	62.04	62.96	58.33
HOG	70.37	68.52	50.93	62.96	62.04
IWBC	68.52	65.74	50.00	64.81	61.11
LAP	70.37	69.44	60.19	64.81	64.81
LBP	62.96	62.96	59.26	61.11	64.81
LDN	67.59	68.52	62.96	<b>67.59</b>	65.74
LDTP	64.81	62.04	62.96	60.19	64.81
LGIP	66.67	60.19	64.81	62.04	62.04
LGP	63.89	63.89	62.96	66.67	60.19
LMP	62.96	63.89	59.26	66.67	62.04
LPQ	66.67	67.59	61.11	66.67	62.04
LTrP	62.96	64.81	62.96	66.67	<b>66.67</b>
MBC	69.44	62.04	50.00	61.11	60.19
MBP	62.96	61.11	59.26	62.96	63.89
PHOG	67.59	62.04	<b>67.59</b>	65.74	61.11
WLD	<b>72.22</b>	<b>69.44</b>	66.67	65.74	62.96

Bolded numbers show the best results among tested feature extractors for a specific classifier (Best results in within a column)

**Table 5** Best axial CN/AD classification accuracy results using pre-trained CNN's

Features	SVM	LDA	QDA	DT	KNN
alexnet	<b>74.07</b>	70.37	<b>62.96</b>	<b>72.22</b>	67.59
darknet19	69.44	64.81	62.04	62.96	61.11
darknet53	73.15	<b>72.22</b>	58.33	68.52	64.81
efficientnet	63.89	60.19	60.19	63.89	60.19
googlenet	69.44	64.81	60.19	69.44	66.67
inc.resnet-v2	67.59	66.67	57.41	62.96	62.96
inception-v3	69.44	68.52	58.33	64.81	64.81
mobilenet-v2	66.67	68.52	59.26	68.52	67.59
nasnetlarge	68.52	68.52	55.56	63.89	62.96
nasnetmobile	69.44	65.74	62.04	65.74	64.81
resnet101	68.52	68.52	59.26	61.11	65.74
resnet18	67.59	62.04	<b>62.96</b>	62.04	60.19
resnet50	67.59	65.74	59.26	63.89	60.19
shufflenet	67.59	65.74	58.33	66.67	<b>69.44</b>
squeezenet	71.30	71.30	59.26	67.59	<b>69.44</b>
vgg16	65.74	65.74	62.04	62.04	65.74
vgg19	71.30	66.67	59.26	63.89	66.67
xception	69.44	68.52	55.56	62.04	60.19

Bolded numbers show the best results among tested feature extractors for a specific classifier (Best results in within a column)

The superior performance of the WLD can be attributed to its capacity to effectively capture intricate patterns present in MRI data.

Table 5 primarily centres around the axial plane, with feature extraction being conducted through the utilisation of pretrained CNNs. The combination of Alexnet and SVM has been found to achieve the highest accuracy rate of 74.07%. This observation suggests that pretrained CNNs, such as Alexnet, demonstrate a high level of efficacy in extracting pertinent features from MRI data, specifically in the axial plane. The modestly superior accuracy observed in CNNs, as compared to histogram descriptors, indicates that CNNs may possess a greater capacity for generalising features in the context of CN/AD classification within this domain.

## 6.2 Coronal plane

Table 6 directs attention towards the coronal plane and once more utilises histogram descriptors for the purpose of classification. The WLD feature demonstrates exceptional performance, achieving an accuracy of 79.63% when utilised in conjunction with SVM and LDA classifiers. The aforementioned high level of accuracy suggests that WLD demonstrates effectiveness not only in the axial plane but also exhibits exceptional performance in the coronal plane. The versatility of this feature in accommodating various planes renders it a suitable option for CN/AD classification.

**Table 6** Best coronal CN/AD classification accuracy results using histogram descriptors

Features	SVM	LDA	QDA	DT	KNN
GDP	62.04	65.74	62.04	62.96	64.81
HOG	63.89	68.52	50.00	62.96	53.70
IWBC	64.81	71.30	50.00	65.74	62.96
LAP	69.44	63.89	66.67	<b>71.30</b>	<b>68.52</b>
LBP	64.81	65.74	60.19	61.11	64.81
LDN	66.67	69.44	65.74	64.81	59.26
LDTP	63.89	65.74	65.74	70.37	60.19
LGIP	70.37	73.15	64.81	63.89	62.04
LGP	73.15	75.93	<b>71.30</b>	65.74	65.74
LMP	64.81	62.96	61.11	64.81	62.04
LPQ	69.44	65.74	64.81	62.96	62.04
LTP	62.96	62.04	59.26	62.04	66.67
MBC	74.07	70.37	53.70	63.89	57.41
MBP	67.59	65.74	60.19	65.74	65.74
PHOG	69.44	66.67	64.81	65.74	63.89
WLD	<b>79.63</b>	<b>79.63</b>	68.52	66.67	<b>68.52</b>

Bolded numbers show the best results among tested feature extractors for a specific classifier (Best results in within a column)

**Table 7** Best coronal CN/AD classification accuracy results using pre-trained cnn's

Features	SVM	LDA	QDA	DT	KNN
alexnet	<b>75.93</b>	<b>73.15</b>	59.26	<b>73.15</b>	65.74
darknet19	70.37	69.44	60.19	63.89	64.81
darknet53	73.15	69.44	60.19	64.81	65.74
efficientnet	65.74	62.04	58.33	67.59	64.81
googlenet	66.67	64.81	<b>65.74</b>	69.44	<b>68.52</b>
inc.resnet-v2	68.52	71.30	<b>65.74</b>	62.04	62.04
inception-v3	74.07	71.30	56.48	68.52	63.89
mobilenet-v2	68.52	69.44	61.11	67.59	63.89
nasnetlarge	71.30	69.44	60.19	67.59	67.59
nasnetmobile	71.30	64.81	59.26	63.89	64.81
resnet101	71.30	70.37	62.04	64.81	61.11
resnet18	75.00	63.89	61.11	64.81	63.89
resnet50	<b>75.93</b>	71.30	60.19	65.74	62.96
shufflenet	69.44	72.22	62.04	67.59	66.67
squeezenet	71.30	69.44	59.26	66.67	62.96
vgg16	70.37	65.74	57.41	64.81	62.96
vgg19	72.22	64.81	61.11	67.59	64.81
xception	71.30	68.52	62.96	67.59	66.67

Bolded numbers show the best results among tested feature extractors for a specific classifier (Best results in within a column)

Table 7 primarily centres its attention on the coronal plane, employing pretrained CNNs for the purpose of feature extraction. The SVM algorithm in conjunction with the AlexNet and ResNet50 models yields a performance of 75.93%, which is the highest level of accuracy. AlexNet has been used in MRI-based cancer classification [70], brain tumour segmentation [71] and Alzheimer’s risk level detection [72], to mention a few. Although the performance is praiseworthy, it falls slightly below the level attained through the use of histogram descriptors. This observation suggests that although CNNs demonstrate effectiveness, they may not possess the same level of adaptability as histogram descriptors such as WLD in the coronal plane.

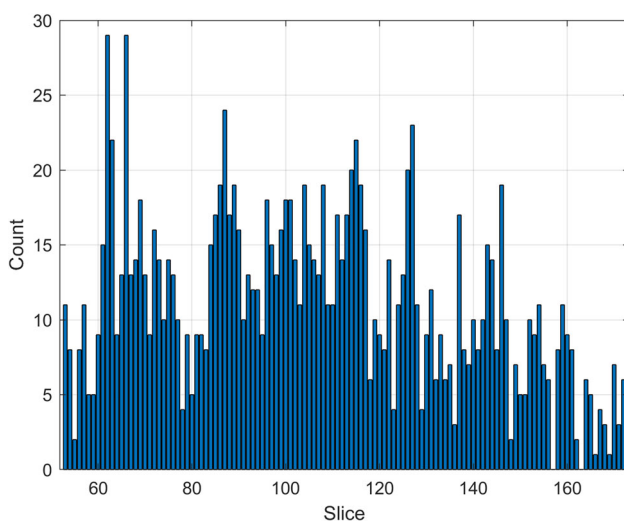


**Fig. 4** Coronal plane: Slice histogram for histogram descriptors. Slices are ordered from the front to the back of the patient’s head

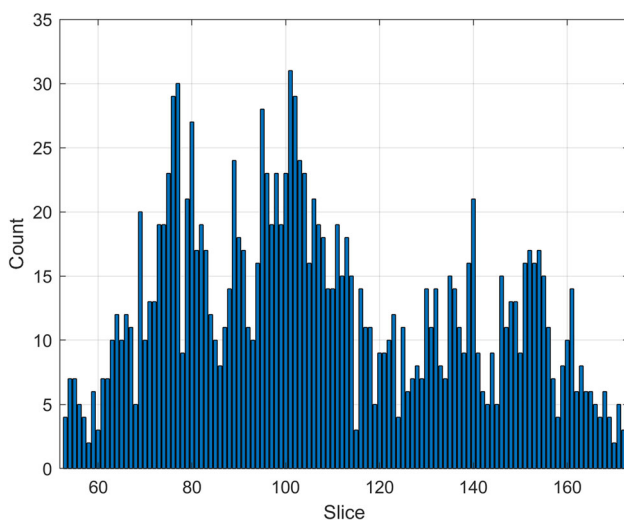


**Fig. 5** Coronal plane: Slice histogram for pre-trained CNN features. Slices are ordered from the front to the back of the patient’s head

When comparing coronal plane slices with the highest model count among the top 10% of the models, both feature variations provide different answers. According to histogram descriptors (Fig. 4), the best slices for classification in the coronal plane are slices numbers 62 and 87, which correspond to the frontal lobe region, and pre-trained CNNs (Fig. 5) offer slice locations at numbers 77 and 101 as the best option for classification, where the frontal and temporal lobes are visible. For example, frontotemporal lobar degeneration (FTLD) and AD are the two most common forms of neurodegenerative dementia [73]. As AD progresses, damage to the frontal lobes may cause a person to have trouble making decisions, planning, or organising [74]. Another peak value at slice number 125 in Fig. 4 according to histogram descriptors can be associated with damage in the right parietal lobe, which causes trouble judging distances in three dimensions, for example, in stairway navigation.

### 6.3 Sagittal plane

The analysis presented in Table 8 examines the sagittal plane and employs histogram descriptors as a means of classification. The combination of the HOG and SVM algorithm yields the highest accuracy rate of 77.78%. This observation implies a change in the predominant influential characteristic when transitioning from axial and coronal planes to sagittal planes. The superior performance exhibited by the HOG method may be attributed to its capacity to effectively capture edge and

**Table 8** Best sagittal CN/AD classification accuracy results using histogram descriptors

Features	SVM	LDA	QDA	DT	KNN
GDP	62.04	62.96	62.04	59.26	61.11
HOG	<b>77.78</b>	68.52	50.00	63.89	58.33
IWBC	70.37	66.67	50.00	65.74	61.11
LAP	61.11	61.11	61.11	<b>73.15</b>	64.81
LBP	66.67	64.81	62.04	67.59	64.81
LDN	63.89	66.67	60.19	63.89	<b>67.59</b>
LDTP	66.67	64.81	<b>65.74</b>	65.74	61.11
LGIP	66.67	66.67	59.26	72.22	62.96
LGP	70.37	<b>75.00</b>	<b>65.74</b>	64.81	65.74
LMP	62.04	62.96	62.96	63.89	64.81
LPQ	63.89	64.81	60.19	64.81	62.96
LTrP	63.89	63.89	59.26	62.04	63.89
MBC	67.59	62.04	50.00	60.19	63.89
MBP	65.74	64.81	62.04	62.96	64.81
PHOG	68.52	68.52	62.96	64.81	61.11
WLD	69.44	69.44	60.19	64.81	62.96

Bolded numbers show the best results among tested feature extractors for a specific classifier (Best results in within a column)

**Table 9** Best sagittal CN/AD classification accuracy results using pre-trained cnn's

Features	SVM	LDA	QDA	DT	KNN
alexnet	72.22	66.67	60.19	65.74	65.74
darknet19	70.37	68.52	59.26	65.74	62.04
darknet53	71.30	68.52	55.56	<b>70.37</b>	<b>71.30</b>
efficientnet	63.89	64.81	58.33	62.04	62.04
googlenet	69.44	<b>69.44</b>	57.41	69.44	66.67
inc.resnet-v2	67.59	65.74	56.48	65.74	65.74
inception-v3	68.52	68.52	58.33	64.81	64.81
mobilenet-v2	75.00	62.04	<b>62.96</b>	62.96	68.52
nasnetlarge	73.15	68.52	57.41	66.67	68.52
nasnetmobile	73.15	65.74	62.04	62.04	65.74
resnet101	75.00	67.59	63.89	62.04	63.89
resnet18	66.67	63.89	60.19	62.96	59.26
resnet50	70.37	63.89	57.41	66.67	65.74
shufflenet	70.37	63.89	55.56	66.67	62.04
squeezenet	<b>75.93</b>	63.89	58.33	68.52	66.67
vgg16	68.52	<b>69.44</b>	59.26	65.74	66.67
vgg19	70.37	64.81	60.19	63.89	60.19
xception	69.44	66.67	61.11	64.81	62.96

Bolded numbers show the best results among tested feature extractors for a specific classifier (Best results in within a column)

texture information, both of which play a crucial role in slices from the sagittal plane.

The primary emphasis in Table 9 is directed towards the sagittal plane, with the utilisation of pretrained CNNs for the purpose of feature extraction. The combination of SqueezeNet and SVM yields the highest accuracy rate of 75.93% and the next best result was achieved by DarkNet53 and KNN with 71.30% accuracy. Although the performance exhibits strength, it is marginally inferior to the results obtained through the utilisation of the HOG feature. This implies that the effectiveness of feature extraction from pretrained CNNs can be subject to variation across different planes, and they may not consistently surpass the performance of traditional histogram descriptors.

The histogram features (Fig. 6) and the pre-trained CNN features (Fig. 7) taken from the sagittal plane show that the sagittal cross section of the temporal lobes can be used as a perspective option for classifying AD. According to the research by Roe et al. [75], cortical asymmetry indicates that the two halves of the brain deteriorate at different rates. They discovered that the left side of the brain shrinks more quickly in AD in the exact same brain regions as in normal ageing.

Among classifiers, the SVM consistently demonstrates its efficacy as a powerful classifier across all tables, thereby highlighting its resilience in effectively handling diverse feature sets and planes. In terms of characteristics, WLD and HOG demonstrate exceptional performance as histogram

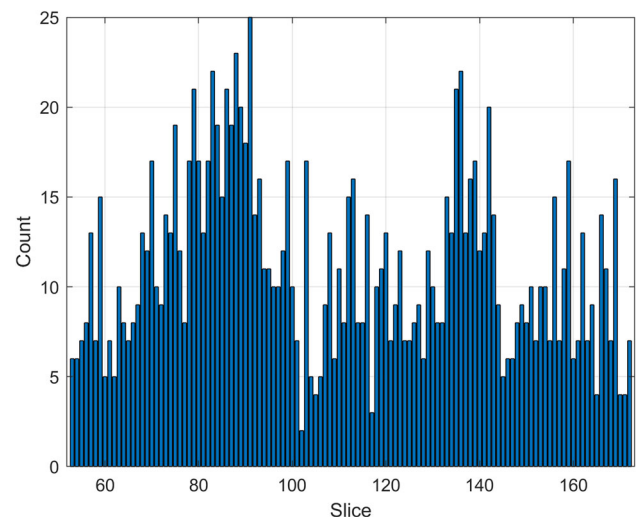


**Fig. 6** Sagittal plane: Slice histogram for histogram descriptors. Peak locations are at slice Nr. 91 and 136. Slices are ordered from the left to the right of the patient's head

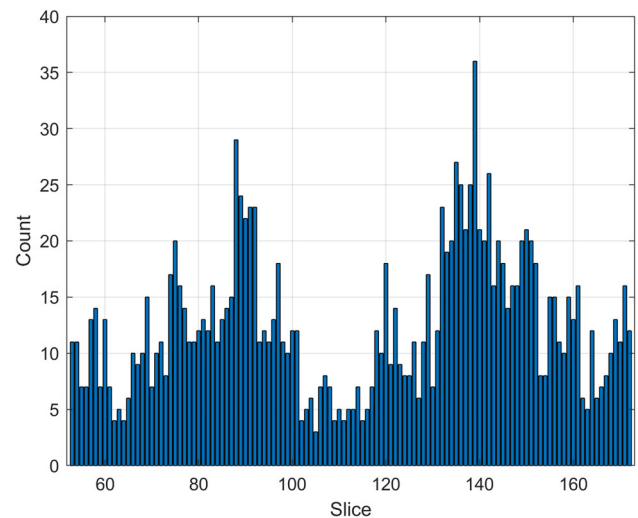


**Fig. 7** Sagittal plane: Slice histogram for pre-trained CNN features. Peak locations are at slice Nr. 88 and 139. Slices are ordered from the left to the right of the patient's head

descriptors, whereas pretrained CNNs such as Alexnet and Resnet50 frequently exhibit notable accuracy levels. Despite this, the effectiveness of these methods varies across different domains. These results may suggest that a combined strategy using both types of features could produce better results for classifying CN and AD.

Table 10 shows comparisons of several CN/AD classification approaches. It can be seen that single-slice classification is comparable with other methods; on the other hand, feature extraction from multiple slices shows better results. Without introducing MRI scan alignment procedures, pre-trained neural networks perform similarly to histogram-based features; therefore, given the availability of data, it would be

**Table 10** Method comparison for CN/AD classification using ADNI MRI dataset

Article	Slice	Feature	Classif.	Acc.
Nayaki and Varghese [54] Split: 75-25 Samples: 200	Axial	GM	SVM	72.00
	Axial	CLBP ALL	SVM	72.00
	Axial	CLBP SM	SVM	74.00
	Axial	CLBP SH	SVM	75.00
	Axial	ALBP	SVM	75.00
	Axial	LBP	SVM	76.00
	Axial	LTP	SVM	78.00
	Axial	CLBP MH	SVM	78.00
	Axial	LPQ MIO	SVM	79.00
	Axial	LGS	SVM	80.00
Ahmed et al. [55] Split: LOOCV Samples: 107	Axial	LQP	SVM	81.00
	Multi	CHF	SVM	85.05
	Multi	SIFT	SVM	79.44
	Multi	SURF	SVM	81.30
	Multi	CSF volume	SVM	78.50
Sarwinda and Bustamam [56] Split: 10-CV Samples: 270	Multi	CHF+CSF	SVM	87.00
	Multi	HOG-TOP	RF	95.80
	Multi	CLBPSM TOP	RF	92.53
Top results Split: 80-20 Samples: 254	Multi	Hybrid	RF	94.70
	Axial	WLD	SVM	72.22
	Coronal	WLD	SVM LDA	79.63
	Sagittal	HOG	SVM	77.78
	Axial	Alexnet	SVM	74.07
	Coronal	Alexnet RasNet50	SVM	75.93
	Sagittal	SqueezeNet	SVM	75.93

more advantageous to look for pre-trained CNNs based on medical images or choose to retrain the chosen CNNs.

## 7 Conclusion

This study's results indicate the potential use of histogram-based local descriptors and feature extraction using pre-trained neural networks for Alzheimer's classification. Among the investigated classifiers, which were SVM, LDA, QDA, DT, and KNN, the best results were achieved using SVM. The three MRI planes were investigated individually, and the following feature types classified with support vector machines are considered the most promising options: in the axial plane, best results were achieved using WLD 72.22% and AlexNet 74.07%, coronal plane, with WLD 79.63%, AlexNet and RasNet50 75.93%, sagittal plane, using histogram of oriented gradients 77.78% and SqueezeNet 75.93%.

The top classification results also indicated the best locations for slice selection in each plane, and the found locations also corresponded to brain regions mentioned in medical

publications in Alzheimer's studies. The best locations for selecting 2D slices from MRI images according to the classification results are as follows: corpus callosum viewed in the axial plane, frontal lobe viewed in the coronal plane, and left and right temporal lobes viewed in the sagittal plane. The future work on this approach will focus on performing slice selection according to aligned and segmented brain regions as reference points.

**Acknowledgements** Data collection and sharing for this project was funded by the Alzheimer's Disease Neuroimaging Initiative (ADNI) (National Institutes of Health Grant U01 AG024904) and DOD ADNI (Department of Defense award number W81XWH-12-2-0012). ADNI is funded by the National Institute on Aging, the National Institute of Biomedical Imaging and Bioengineering, and through generous contributions from the following: AbbVie, Alzheimer's Association; Alzheimer's Drug Discovery Foundation; Araclon Biotech; BioClinica, Inc.; Biogen; Bristol-Myers Squibb Company; CereSpir, Inc.; Cogstate; Eisai Inc.; Elan Pharmaceuticals, Inc.; Eli Lilly and Company; EuroImmun; F. Hoffmann-La Roche Ltd and its affiliated company Genentech, Inc.; Fujirebio; GE Healthcare; IXICO Ltd.; Janssen Alzheimer Immunotherapy Research & Development, LLC.; Johnson & Johnson Pharmaceutical Research & Development LLC.; Lumosity; Lundbeck; Merck & Co., Inc.; Meso Scale Diagnostics, LLC.; NeuroRx Research; Neurotrack Technologies; Novartis Pharmaceuticals

Corporation; Pfizer Inc.; Piramal Imaging; Servier; Takeda Pharmaceutical Company; and Transition Therapeutics. The Canadian Institutes of Health Research is providing funds to support ADNI clinical sites in Canada. Private sector contributions are facilitated by the Foundation for the National Institutes of Health ([www.fnih.org](http://www.fnih.org)). The grantee organisation is the Northern California Institute for Research and Education, and the study is coordinated by the Alzheimer's Therapeutic Research Institute at the University of Southern California. ADNI data are disseminated by the Laboratory for Neuro Imaging at the University of Southern California.

**Author Contributions** E. Avots developed the methodology and conducted experiments. A. A. Jafari worked on data preprocessing and conducted experiments. E. Avots, A. A. Jafari, C. Ozcinar wrote the main manuscript text. C. Ozcinar was the main article editor. G. Anbarjafari guided the research process. Alzheimer's Disease Neuroimaging Initiative (ADNI) provided the MRI data and ADNI Data and Publications Committee (DPC) conducted preliminary revision. All authors reviewed the manuscript.

**Funding** None.

**Availability of data and materials** The ADNI dataset can be obtained by going through the application process, which includes acceptance of the Data Use Agreement and submission of an online application form that can be found at <https://adni.loni.usc.edu/>.

## Declarations

**Conflict of interest** The authors declare no competing interests.

**Ethical approval** ADNI conducts research according to Good Clinical Practice guidelines, US 21CFR Part 50- Protection of Human Subjects, and Part 56 - Institutional Review Boards (IRBs) / Research Ethics Boards (REBs), and pursuant to state and federal HIPAA regulations.

## References

- International, A.D.: Dementia statistics (2023)
- Afzal, S., Maqsood, M., Khan, U., Mehmood, I., Nawaz, H., Aadil, F., Song, O.-Y., Yunyoung, N.: Alzheimer disease detection techniques and methods: a review (2021)
- Beheshti, I., Maikusa, N., Daneshmand, M., Matsuda, H., Demirel, H., Anbarjafari, G., et al.: Classification of alzheimer's disease and prediction of mild cognitive impairment conversion using histogram-based analysis of patient-specific anatomical brain connectivity networks. *J. Alzheimer's Dis.* **60**(1), 295–304 (2017)
- Beheshti, I., Maikusa, N., Matsuda, H., Demirel, H., Anbarjafari, G., et al.: Histogram-based feature extraction from individual gray matter similarity-matrix for alzheimer's disease classification. *J. Alzheimer's Dis.* **55**(4), 1571–1582 (2017)
- Elshatoury, H., Avots, E., Anbarjafari, G., Initiative, A.D.N., et al.: Volumetric histogram-based alzheimer's disease detection using support vector machine. *J. Alzheimer's Dis.* **72**(2), 515–524 (2019)
- Sunderland, T., Hill, J.L., Mellow, A.M., Lawlor, B.A., Gundersheimer, J., Newhouse, P.A., Grafman, J.H.: Clock drawing in alzheimer's disease: a novel measure of dementia severity. *J. Am. Geriatr. Soc.* **37**(8), 725–729 (1989)
- Avots, E., Jermakovs, K., Bachmann, M., Päske, L., Ozcinar, C., Anbarjafari, G.: Ensemble approach for detection of depression using eeg features. *Entropy* **24**(2), 211 (2022)
- Arafa, D.A., Moustafa, H.E.-D., Ali-Eldin, A.M., Ali, H.A.: Early detection of alzheimer's disease based on the state-of-the-art deep learning approach: a comprehensive survey. *Multimed. Tools Appl.* **81**(17), 23735–23776 (2022)
- Aktas, K., Ignjatovic, V., Ilic, D., Marjanovic, M., Anbarjafari, G.: Deep convolutional neural networks for detection of abnormalities in chest x-rays trained on the very large dataset. *Signal Image Video Process.* **17**(4), 1035–1041 (2023)
- Sham, A.H., Tikka, P., Lamas, D., Anbarjafari, G.: Automatic reaction emotion estimation in a human-human dyadic setting using deep neural networks. *Signal Image Video Process.* **17**(2), 527–534 (2023)
- Lu, J., Liong, V.E., Zhou, X., Zhou, J.: Learning compact binary face descriptor for face recognition. *IEEE Trans. Pattern Anal. Mach. Intell.* **37**(10), 2041–2056 (2015)
- Turan, C., Lam, K.-M.: Histogram-based local descriptors for facial expression recognition (fer): a comprehensive study. *J. Vis. Commun. Image Represent.* **55**, 331–341 (2018)
- Kumar, T.S., Rajesh, K.N., Maheswari, S., Kanhangad, V., Acharya, U.R.: Automated schizophrenia detection using local descriptors with eeg signals. *Eng. Appl. Artif. Intell.* **117**, 105602 (2023)
- Ojala, T., Pietikainen, M., Maenpää, T.: Multiresolution gray-scale and rotation invariant texture classification with local binary patterns. *IEEE Trans. Pattern Anal. Mach. Intell.* **24**(7), 971–987 (2002)
- Dalal, N., Triggs, B.: Histograms of oriented gradients for human detection. In: 2005 IEEE Computer Society Conference on Computer Vision and Pattern Recognition (CVPR'05), vol. 1, pp. 886–893. IEEE (2005)
- Bosch, A., Zisserman, A., Muñoz, X.: Representing shape with a spatial pyramid kernel. In: Proceedings of the 6th ACM International Conference on Image and Video Retrieval, pp. 401–408 (2007)
- Ojansivu, V., Heikkilä, J.: Blur insensitive texture classification using local phase quantization. In: Image and Signal Processing: 3rd International Conference, ICISP 2008. Cherbourg-Octeville, France, July 1-3, 2008. Proceedings 3, pp. 236–243. Springer (2008)
- Dhall, A., Asthana, A., Goecke, R., Gedeon, T.: Emotion recognition using phog and lpq features. In: 2011 IEEE International Conference on Automatic Face & Gesture Recognition (FG), pp. 878–883. IEEE (2011)
- Macin, G., Tasci, B., Tasci, I., Faust, O., Barua, P.D., Dogan, S., Tuncer, T., Tan, R.-S., Acharya, U.R.: An accurate multiple sclerosis detection model based on exemplar multiple parameters local phase quantization: Exmplpq. *Appl. Sci.* **12**(10), 4920 (2022)
- Mohammad, T., Ali, M.L.: Robust facial expression recognition based on local monotonic pattern (lmp). In: 14th International Conference on Computer and Information Technology (ICCIT 2011), pp. 572–576. IEEE (2011)
- Jabid, T., Chae, O.: Local transitional pattern: A robust facial image descriptor for automatic facial expression recognition. In: Proceedings of the International Conference on Computer Convergence Technology, Seoul, Korea, pp. 333–344 (2011)
- Jabid, T., Chae, O.: Facial expression recognition based on local transitional pattern. *Int. Inf. Inst. (Tokyo) Inf.* **15**(5), 2007 (2012)
- Yang, M., Zhang, L., Shiu, S.C.-K., Zhang, D.: Monogenic binary coding: an efficient local feature extraction approach to face recognition. *IEEE Trans. Inf. Forensics Secur.* **7**(6), 1738–1751 (2012)
- Lu, J., Liong, V.E., Zhou, J.: Cost-sensitive local binary feature learning for facial age estimation. *IEEE Trans. Image Process.* **24**(12), 5356–5368 (2015)
- Zhou, L., Wang, H.: Local gradient increasing pattern for facial expression recognition. In: 2012 19th IEEE International Conference on Image Processing, pp. 2601–2604. IEEE (2012)

26. Rivera, A.R., Castillo, J.R., Chae, O.O.: Local directional number pattern for face analysis: face and expression recognition. *IEEE Trans. Image Process.* **22**(5), 1740–1752 (2012)
27. Ahmed, F.: Gradient directional pattern: a robust feature descriptor for facial expression recognition. *Electron. Lett.* **48**(19), 1203–1204 (2012)
28. Chu, W.: Facial expression recognition based on local binary pattern and gradient directional pattern. In: 2013 IEEE International Conference on Green Computing and Communications and IEEE Internet of Things and IEEE Cyber, Physical and Social Computing, pp. 1458–1462. IEEE (2013)
29. Rao, R.V., Prasad, T.: A new optimized hybrid local lifting wavelet co-occurrence texture pattern for content based medical image retrieval. *Int. J. Online Biomed. Eng.* **17**(11) (2021)
30. Li, S., Gong, D., Yuan, Y.: Face recognition using weber local descriptors. *Neurocomputing* **122**, 272–283 (2013)
31. Liu, S., Zhang, Y., Liu, K.: Facial expression recognition under partial occlusion based on weber local descriptor histogram and decision fusion. In: Proceedings of the 33rd Chinese Control Conference, pp. 4664–4668. IEEE (2014)
32. Islam, M.S., Auwatanamo, S.: Facial expression recognition using local arc pattern. *Trends Appl. Sci. Res.* **9**(2), 113 (2014)
33. Islam, M.S.: Local gradient pattern—a novel feature representation for facial expression recognition. *J. AI Data Min.* **2**(1), 33–38 (2014)
34. Bashar, F., Khan, A., Ahmed, F., Kabir, M.H.: Robust facial expression recognition based on median ternary pattern (mtp). In: 2013 International Conference on Electrical Information and Communication Technology (EICT), pp. 1–5. IEEE (2014)
35. Rivera, A.R., Castillo, J.R., Chae, O.: Local directional texture pattern image descriptor. *Pattern Recognit. Lett.* **51**, 94–100 (2015)
36. Yang, B.-Q., Zhang, T., Gu, C.-C., Wu, K.-J., Guan, X.-P.: A novel face recognition method based on iwld and iwbc. *Multimed. Tools Appl.* **75**, 6979–7002 (2016)
37. Russakovsky, O., Deng, J., Su, H., Krause, J., Satheesh, S., Ma, S., Huang, Z., Karpathy, A., Khosla, A., Bernstein, M., et al.: Imagenet large scale visual recognition challenge. *Int. J. Comput. Vis.* **115**, 211–252 (2015)
38. Greenspan, H., Van Ginneken, B., Summers, R.M.: Guest editorial deep learning in medical imaging: overview and future promise of an exciting new technique. *IEEE Trans. Med. Imaging* **35**(5), 1153–1159 (2016)
39. Ashraf, A., Naz, S., Shirazi, S.H., Razzak, I., Parsad, M.: Deep transfer learning for alzheimer neurological disorder detection. *Multimed. Tools Appl.* 1–26 (2021)
40. Suk, H.-I., Lee, S.-W., Shen, D., Initiative, A.D.N., et al.: Hierarchical feature representation and multimodal fusion with deep learning for ad/mci diagnosis. *NeuroImage* **101**, 569–582 (2014)
41. Krizhevsky, A., Sutskever, I., Hinton, G.E.: Imagenet classification with deep convolutional neural networks. In: Proceedings of the 25th International Conference on Neural Information Processing Systems—Volume 1, NIPS’12, (Red Hook, NY, USA), pp. 1097–1105. Curran Associates Inc. (2012)
42. Simonyan, K., Zisserman, A.: Very deep convolutional networks for large-scale image recognition. [arXiv:1409.1556](https://arxiv.org/abs/1409.1556) (2014)
43. Szegedy, C., Liu, W., Jia, Y., Sermanet, P., Reed, S., Anguelov, D., Erhan, D., Vanhoucke, V., Rabinovich, A.: Going deeper with convolutions. In: Proceedings of the IEEE Conference on Computer Vision and Pattern Recognition, pp. 1–9 (2015)
44. Szegedy, C., Vanhoucke, V., Ioffe, S., Shlens, J., Wojna, Z.: Rethinking the inception architecture for computer vision. In: Proceedings of the IEEE Conference on Computer Vision and Pattern Recognition, pp. 2818–2826 (2016)
45. He, K., Zhang, X., Ren, S., Sun, J.: Deep residual learning for image recognition. In: Proceedings of the IEEE Conference on Computer Vision and Pattern Recognition, pp. 770–778 (2016)
46. Iandola, F.N., Han, S., Moskewicz, M.W., Ashraf, K., Dally, W.J., Keutzer, K.: Squeezenet: Alexnet-level accuracy with 50x fewer parameters and < 0.5 mb model size. [arXiv:1602.07360](https://arxiv.org/abs/1602.07360) (2016)
47. Szegedy, C., Ioffe, S., Vanhoucke, V., Alemi, A.: Inception-v4, inception-resnet and the impact of residual connections on learning. In: Proceedings of the AAAI Conference on Artificial Intelligence, vol. 31 (2017)
48. Chollet, F.: Xception: deep learning with depthwise separable convolutions. In: Proceedings of the IEEE Conference on Computer Vision and Pattern Recognition, pp. 1251–1258 (2017)
49. Redmon, J., Farhadi, A.: Yolo9000: better, faster, stronger. In: Proceedings of the IEEE Conference on Computer Vision and Pattern Recognition, pp. 7263–7271 (2017)
50. Zhang, X., Zhou, X., Lin, M., Sun, J.: Shufflenet: an extremely efficient convolutional neural network for mobile devices. In: Proceedings of the IEEE Conference on Computer Vision and Pattern Recognition, pp. 6848–6856 (2018)
51. Zoph, B., Vasudevan, V., Shlens, J., Le, Q.V.: Learning transferable architectures for scalable image recognition. In: Proceedings of the IEEE Conference on Computer Vision and Pattern Recognition, pp. 8697–8710 (2018)
52. Sandler, M., Howard, A., Zhu, M., Zhmoginov, A., Chen, L.-C.: Mobilenetv2: inverted residuals and linear bottlenecks. In: Proceedings of the IEEE Conference on Computer Vision and Pattern Recognition, pp. 4510–4520 (2018)
53. Tan, M., Le, Q.: Efficientnet: rethinking model scaling for convolutional neural networks. In: International Conference on Machine Learning, pp. 6105–6114. PMLR (2019)
54. Nayaki, K.S., Varghese, A.: Alzheimer’s detection at early stage using local measures on mri: a comparative study on local measures. In: 2014 International Conference on Data Science & Engineering (ICDSE), pp. 224–227. IEEE (2014)
55. Ben Ahmed, O., Benois-Pineau, J., Allard, M., Ben Amar, C., Catheline, G., Initiative, A.D.N.: Classification of alzheimer’s disease subjects from mri using hippocampal visual features. *Multimed. Tools Appl.* **74**, 1249–1266 (2015)
56. Sarwinda, D., Bustamam, A.: 3d-hog features–based classification using mri images to early diagnosis of alzheimer’s disease. In: 2018 IEEE/ACIS 17th International Conference on Computer and Information Science (ICIS), pp. 457–462. IEEE (2018)
57. Altaf, T., Anwar, S.M., Gul, N., Majeed, M.N., Majid, M.: Multi-class alzheimer’s disease classification using image and clinical features. *Biomed. Signal Process. Control* **43**, 64–74 (2018)
58. Cao, P., Gao, J., Zhang, Z.: Multi-view based multi-model learning for mci diagnosis. *Brain Sci.* **10**(3), 181 (2020)
59. Cohen, D.S., Carpenter, K.A., Jarrell, J.T., Huang, X., Initiative, A.D.N., et al.: Deep learning-based classification of multi-categorical alzheimer’s disease data. *Curr. Neurobiol.* **10**(3), 141 (2019)
60. Basaia, S., Agosta, F., Wagner, L., Canu, E., Magnani, G., Santangelo, R., Filippi, M., Initiative, A.D.N., et al.: Automated classification of alzheimer’s disease and mild cognitive impairment using a single mri and deep neural networks. *NeuroImage Clin.* **21**, 101645 (2019)
61. Kumar, P.S., Dharun, V.: A study of mri segmentation methods in automatic brain tumor detection. *Int. J. Eng. Technol.* **8**(2), 609–614 (2016)
62. Gudadhe, S.S., Thakare, A.D., Oliva, D.: Classification of intracranial hemorrhage ct images based on texture analysis using ensemble-based machine learning algorithms: A comparative study. *Biomed. Signal Process. Control* **84**, 104832 (2023)
63. Stanley, B.F., Franklin, S.W.: Effective feature extraction for cerebral microbleed detection using edge emphasized weber maximum directional co-occurrence matrix. *J. Ambient Intell. Humaniz. Comput.* 1–14 (2022)

64. Saif, A., Imtiaz, T., Shahnaz, C., Zhu, W.-P., Ahmad, M.O.: Exploiting cascaded ensemble of features for the detection of tuberculosis using chest radiographs. *IEEE Access* **9**, 112388–112399 (2021)
65. Bramarambika, M.: Brain tumor classification for mr images using hybrid glcm-ldtp-le-net feature extraction and bi-lstm model. *Int. J. Intell. Eng. Syst.* **15**(2) (2022)
66. Mwadulo, M.W.: Alocal directional ternary pattern texture descriptor for mammographic breast cancer classification. PhD thesis, MMUST (2020)
67. Uplaonkar, D.S., Virupakshappa, Patil, N.: Modified otsu thresholding based level set and local directional ternary pattern technique for liver tumor segmentation. *Int. J. Syst. Assur. Eng. Manag.* 1–11 (2022)
68. Hassan, W.A., Ali, Y.H., Ibrahim, N.J.: A survey of latest techniques in medical image classification. In: 2021 International Conference on Communication & Information Technology (ICICT), pp. 68–73. IEEE (2021)
69. Khasawneh, R.R., Abu-El-Rub, E., Alzu'bi, A., Abdelhady, G.T., Al-Soudi, H.S.: Corpus callosum anatomical changes in alzheimer patients and the effect of acetylcholinesterase inhibitors on corpus callosum morphometry. *PLoS One* **17**(7), e0269082 (2022)
70. Li, J., Wang, P., Li, Y., Zhou, Y., Liu, X., Luan, K.: Transfer learning of pre-trained inception-v3 model for colorectal cancer lymph node metastasis classification. In: 2018 IEEE International Conference on Mechatronics and Automation (ICMA), pp. 1650–1654. IEEE (2018)
71. Shoaib, M., Sayed, N.: Yolo object detector and inception-v3 convolutional neural network for improved brain tumor segmentation. *Traitement Du Signal* **39**(1) (2022)
72. Singh, R., Sharma, N., Gupta, R.: Detection of alzheimer's risk level using inception v3 transfer learning model. in: 2023 International Conference on Distributed Computing and Electrical Circuits and Electronics (ICDCECE), pp. 1–6. IEEE (2023)
73. Li, P., Quan, W., Wang, Z., Liu, Y., Cai, H., Chen, Y., Wang, Y., Zhang, M., Tian, Z., Zhang, H., et al.: Early-stage differentiation between alzheimer's disease and frontotemporal lobe degeneration: Clinical, neuropsychology, and neuroimaging features. *Front. Aging Neurosci.* **14**, 981451 (2022)
74. Lindau, M., Almkvist, O., Kushi, J., Boone, K., Johansson, S., Wahlund, L., Cummings, J., Miller, B.: First symptoms-frontotemporal dementia versus alzheimer's disease. *Dement. Geriatr. Cogn. Disord.* **11**(5), 286–293 (2000)
75. Roe, J.M., Vidal-Piñeiro, D., Sørensen, Ø., Brandmaier, A.M., Düzel, S., Gonzalez, H.A., Kievit, R.A., Knights, E., Kühn, S., Lindenberger, U., et al.: Asymmetric thinning of the cerebral cortex across the adult lifespan is accelerated in alzheimer's disease. *Nat. Commun.* **12**(1), 721 (2021)

**Publisher's Note** Springer Nature remains neutral with regard to jurisdictional claims in published maps and institutional affiliations.

Springer Nature or its licensor (e.g. a society or other partner) holds exclusive rights to this article under a publishing agreement with the author(s) or other rightsholder(s); author self-archiving of the accepted manuscript version of this article is solely governed by the terms of such publishing agreement and applicable law.